

Article

Selective 5-Hydroxymethylfurfural Hydrogenolysis to 2,5-Dimethylfuran over Bimetallic Pt-FeO_x/AC Catalysts

Yongjie Xin¹, Sichan Li², Haiyong Wang³, Lungang Chen³, Shuang Li^{1,*} and Qiyong Liu^{3,*}¹ School of Chemical Engineering, Northwest University, Xi'an 710069, China; xinyongjie@stumail.nwu.edu.cn² Nano Science and Technology Institute, University of Science and Technology of China, Suzhou 215123, China; lisc@ms.giec.ac.cn³ Guangzhou Institute of Energy Conversion, Chinese Academy of Sciences, Guangzhou 510640, China; wanghy@ms.giec.ac.cn (H.W.); chenlg1981@ms.giec.ac.cn (L.C.)

* Correspondence: shuangli@nwu.edu.cn (S.L.); liuqy@ms.giec.ac.cn (Q.L.); Tel.: +86-186-2960-0811 (S.L.); +86-138-2649-5503 (Q.L.)

Abstract: The selective hydrogenolysis of 5-hydroxymethylfurfural (HMF) platform molecule to 2,5-dimethylfuran (DMF) has attracted increasing attention due to its broad range of applications. However, HMF, with multiple functional groups, produces various byproducts, hindering its use on an industrial scale. Herein, a bimetallic Pt-FeO_x/AC catalyst with low Pt and FeO_x loadings for selective HMF hydrogenolysis to DMF was prepared by incipient wetness impregnation. The structures and properties of different catalysts were characterized by XRD, XPS, TEM, ICP-OES and Py-FTIR techniques. The addition of FeO_x enhanced Pt dispersion and the Lewis acidic site density of the catalysts, and was found to be able to inhibit C=C hydrogenation, thereby improving DMF yield. Moreover, the presence of Pt promoted the reduction of iron oxide, creating a strong interaction between Pt and FeO_x. This synergistic effect originated from the activation of the C–O bond over FeO_x species followed by hydrogenolysis over the adjacent Pt, and played a critical role in hydrogenolysis of HMF to DMF, achieving a yield of 91% under optimal reaction conditions. However, the leaching of Fe species caused a metal–acid imbalance, which led to an increase in ring hydrogenation products.

Keywords: 5-hydroxymethylfurfural; 2,5-dimethylfuran; hydrogenolysis; Pt-FeO_x/AC; synergistic effect



Citation: Xin, Y.; Li, S.; Wang, H.; Chen, L.; Li, S.; Liu, Q. Selective 5-Hydroxymethylfurfural Hydrogenolysis to 2,5-Dimethylfuran over Bimetallic Pt-FeO_x/AC Catalysts. *Catalysts* **2021**, *11*, 915. <https://doi.org/10.3390/catal11080915>

Academic Editor:
Federica Menegazzo

Received: 3 July 2021
Accepted: 24 July 2021
Published: 28 July 2021

Publisher's Note: MDPI stays neutral with regard to jurisdictional claims in published maps and institutional affiliations.



Copyright: © 2021 by the authors. Licensee MDPI, Basel, Switzerland. This article is an open access article distributed under the terms and conditions of the Creative Commons Attribution (CC BY) license (<https://creativecommons.org/licenses/by/4.0/>).

1. Introduction

With the development of technology, the continued exploitation of fossil fuels is causing more and more environmental problems, such as global warming owing to massive greenhouse gas emissions [1–4]. Biomass is extensively utilized in the production of fuels and high value-added chemicals based on its abundant storage, wide distribution and renewability [5]. There is a large amount of oxygen in molecules derived from biomass, to which the process of hydrodeoxygenation is often applied [6]. The compound 5-hydroxymethylfurfural (HMF), which can be produced by hydrolysis of cellulose by using an acid catalyst, is considered one of the ten most important biomass platform molecules [7]. Among HMF derivatives, 2,5-dimethylfuran (DMF) has been widely studied as a nontoxic gasoline additive due to its high octane number (RON = 119), low oxygen content (O/C = 0.17), ideal boiling point (92–94 °C), high energy density (30 kJ·cm⁻³) and poor water solubility (2.3 g·L⁻¹) [8–11].

Previous studies have found that noble-metal catalysts (Ru [12,13], Pt [14,15], and Pd [16]) exhibited excellent catalytic performance in the selective hydrogenation of HMF to DMF. Due to the high cost of precious metals, a large number of nonprecious metal-based catalysts (Ni [17,18], Co [19], Cu [20] etc.) have also been extensively studied. However, the majority of these catalytic systems require a large amount of metal loading

and harsh reaction conditions such as high temperature and high H₂ pressure. It has recently been found that bimetallic catalysts with metal–metal bonds and electronic interactions demonstrate superior catalytic hydrogenation performance than single metal catalysts, especially the combination of precious metals and transition metals. For example, Luo and coworkers prepared Pt-Ni, Pt-Zn and Pt-Cu alloyed catalysts using carbon as a support for HMF hydrogenolysis, and achieved DMF yields of 98%, 97% and 96%, respectively, at a pressure of 3.3 MPa H₂ and between 160 and 200 °C [21]. Bimetallic catalysts such as Ru-Co/SiO₂ [22], PtCo@HCS [23] and Cu–Pd@C [6] etc. have also obtained more than 95% yields of DMF. Moreover, it has been reported in the literature that DMF can obtain a better yield in the presence of Lewis acid, HCl [24], H₂SO₄, formic acid etc., although the presence of a corrosive liquid acid gives rise to the need for neutralization after the reaction, resulting in an environmentally unfriendly process [25,26]. The study found that the addition of transition metal additives which can easily form Lewis acid under a hydrogen atmosphere is beneficial to the formation of DMF [27]. For example, Yang et al. prepared Ru–MoO_x/C catalysts and obtained a 79.4% yield of DMF due to the synergistic effect between metallic Ru and acidic MoO_x species, which showed effective hydrogenation on Ru and accelerated hydrogenolysis over MoO_x [28].

It has been accepted that active metal sites for H₂ dissociation and Lewis acidic sites for the activation of C=O bonds are required for selective hydrodeoxygenation of HMF to DMF by catalysis. In particular, the Lewis acidic sites which adsorb substrates via an end-on mode of the O atom are the prerequisite to achieve high chemo-selectivity [29]. Pt has extremely high hydrogenation activity with uncontrolled rate, attributed to a large radial expansion of the d orbitals [30]. Therefore, it is easy to produce excessive hydrogenation products, and the introduction of an appropriate additive is necessary to improve chemo-selectivity. Fe is often used as an additive or support due to its poor catalytic activity; however, the FeO_x species with a certain acidity and oxophilic nature facilitate the adsorption of the furan ring [31]. The Pt–FeO_x interface, containing an ensemble of Pt and Fe oxides or oxygen vacancies at the contacting boundary of Pt–FeO_x, has been identified as the most efficient active site for a number of selective hydrogenation/oxidation reactions [32]. For example, Wang et al. confirmed by theoretical calculations and temperature programmed desorption (TPD) experiments that the C=O bond of furfural was more strongly bound to the surface on Fe/Pt(111) compared to Pt(111), which is more conducive to C=O bond cleavage [33]. In addition, Zanuttini et al. investigated the hydrodeoxygenation of furfural compounds in the gas phase at 573 K using FePt/SiO₂, and found that the combination of Fe and Pt resulted in higher reaction rates and reduced coke formation [34]. However, there is little research on the synergistic effect of Pt and the acid additive FeO_x in the catalytic hydrodeoxygenation of HMF.

In this work, bimetallic Pt and FeO_x containing catalysts with an activated carbon support (Pt-FeO_x/AC) were prepared via incipient wetness impregnation. TEM, XRD, XPS, ICP-OES and Py-FTIR were utilized to characterize the structures of the catalysts and the synergistic effect of Pt and FeO_x species. Under optimized condition, the 0.5% Pt-2% FeO_x/AC catalyst achieved 91.1% DMF yield in 6 h at 180 °C. A plausible reaction pathway and synergistic effect between metallic Pt and acidic FeO_x are proposed in this paper.

2. Results and Discussion

2.1. Catalyst Characterization

The XRD patterns of catalysts are shown in Figure 1. Several diffraction peaks assigned to Fe₃O₄ at 2θ = 30.0° (220), 35.3° (311), 43.0° (400), 56.9° (511) and 62.5° (440) were clearly observed [35,36]. In addition, the characteristic peak at 2θ = 33.1° was attributed to the (104) diffraction of α-Fe₂O₃ [37]. No diffraction peaks of Pt were observed in the XRD patterns of catalysts, but ICP was performed to determine the existence of Pt, as shown in Table 1. In addition, the Pt and Fe contents of different catalysts were slightly lower than the theoretical values by ICP-OES analysis. This implies that the Pt particles, which were too small to be detected by XRD measurement, were highly dispersed on the AC.

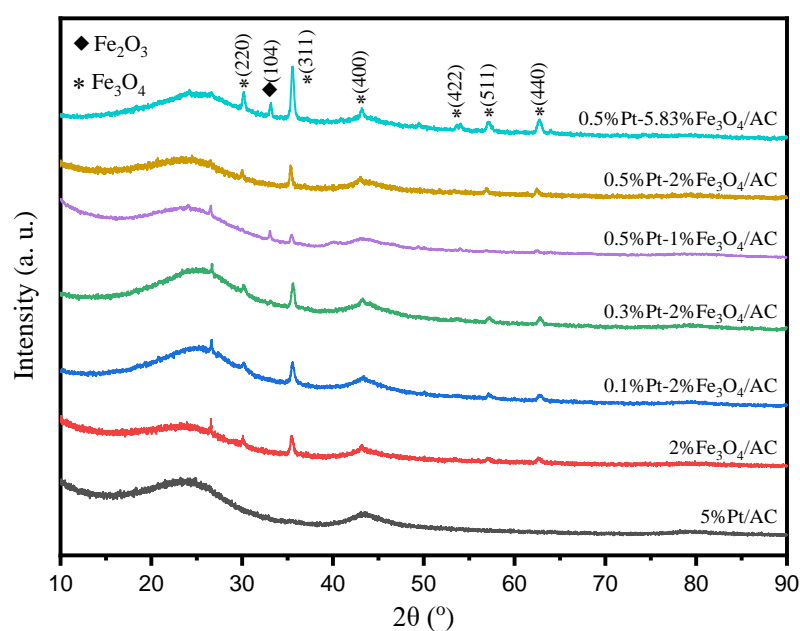


Figure 1. XRD patterns of different catalysts.

Table 1. Physicochemical properties of different Pt-FeO_x/AC catalysts.

Catalysts	d_{Pt} ^a (nm)	D_{Pt} ^b	Pt ^c (wt %)	Pt _{sur} ^d (μmol/g)	Fe ^c (wt %)	Lewis Acidic Sites ^e (μmol/g)	Fe ²⁺ /Fe ³⁺ ^f	Pt ²⁺ /Pt ⁰ ^f
0.5%Pt/AC	4.7 ± 1.32	0.24	0.35	4.3	-	15.6	-	0.61
2%FeO _x /AC	-	-	-	-	1.9	16.5	0.25	-
0.1%Pt-2%FeO _x /AC	1.7 ± 0.25	0.67	0.06	2.1	1.6	22.5	0.31	0.98
0.3%Pt-2%FeO _x /AC	1.8 ± 0.26	0.63	0.21	6.8	1.5	26.2	0.47	0.91
0.5%Pt-1%FeO _x /AC	4.3 ± 1.17	0.26	0.45	6.0	1.0	20.9	0.99	0.73
0.5%Pt-2%FeO _x /AC	2.8 ± 0.67	0.40	0.36	7.4	1.6	29.9	0.89	0.82
Used-1st 0.5%Pt-2%FeO _x /AC	3.3 ± 1.03	0.34	0.35	6.1	1.2	-	0.52	0.14
0.5%Pt-5.83%FeO _x /AC	4.6 ± 1.26	0.25	0.33	4.2	4.6	16.4	0.66	1.23

^a d_{Pt} represents the mean diameter of the Pt particle measured by TEM images. ^b D_{Pt} represents the dispersion of the Pt particle, estimated by the previous reference [38]. ^c Pt (wt %) and Fe (wt %) represent the Pt and Fe loading from ICP analysis. ^d Pt_{sur} (μmol/g) represents the density of Pt on the metal particle surface, which is calculated by $D_{Pt} \times Pt$ (wt %)/ M_{Pt} (M_{Pt} , relative atomic mass of Pt). ^e Lewis acidic sites (μmol/g) represents the density of Lewis acidic sites from Py-FTIR. ^f Fe²⁺/Fe³⁺ and Pt²⁺/Pt⁰ represent the atomic ratio via peak fitting from XPS analysis.

The metallic Pt and Fe oxide particles in the 0.5% Pt-2% FeO_x/AC were uniformly dispersed on the activated carbon (Figure 2a); the average size of the Pt nanoparticles was about 2.8 nm (Figure 2c). As shown in Figure 2b, lattice spacings of 0.224 nm and 0.254 nm were observed, which were recognized as Pt (111) and Fe₃O₄ (311) [39,40], respectively. The EDS mapping profiles revealed that Pt, Fe and O were uniformly distributed on the activated carbon (Figure 2d–g). A TEM image and particle size distribution histogram of the 0.5% Pt/AC catalyst are also shown in Figure 3. It can be seen that the average size of the Pt nanoparticles was about 4.7 nm, indicating that the addition of FeO_x greatly enhanced the Pt dispersion. Moreover, Figure S1 shows TEM images and particle size distributions of other catalysts with different Pt and Fe loadings. In addition, the dispersion of Pt was estimated from the average particle size obtained by TEM, and the number of active sites of Pt on the catalyst surface was calculated by combining the real Pt content and the dispersion of Pt, as shown in Table 1.

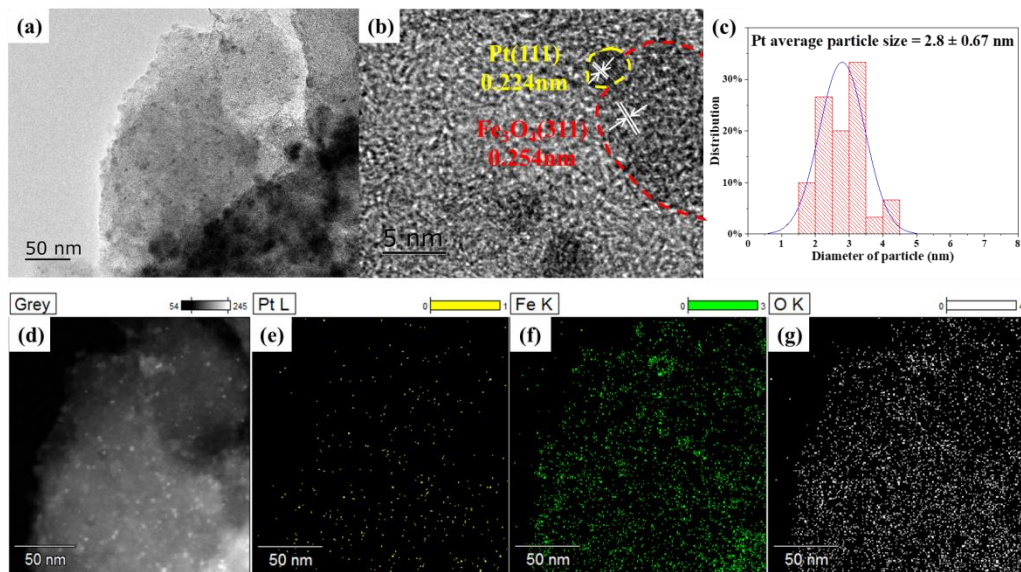


Figure 2. (a,b) TEM images with low and high magnification, respectively; (c) particle size distribution histogram; (d–g) EDS mapping profiles for (e) Pt, (f) Fe, and (g) O of 0.5% Pt-2% FeO_x/AC catalyst.

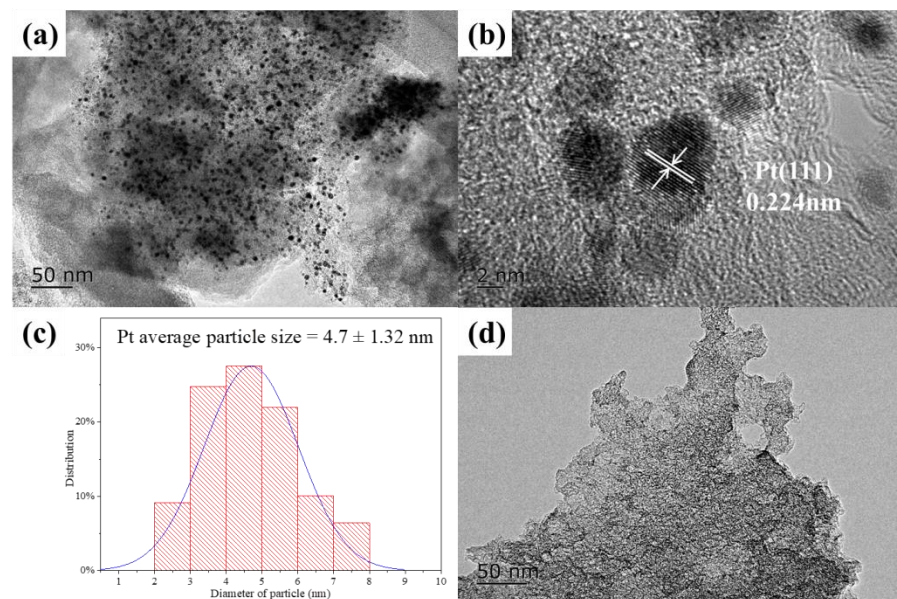


Figure 3. TEM images of 0.5% Pt/AC (a,b), 2% FeO_x/AC (d), and particle size distribution histogram of 0.5% Pt/AC (c).

We performed an XPS analysis to investigate the surface element composition and chemical valence state. As shown in Figure 4a, the Fe 2p_{3/2} peaks at 710.1 and 711.5 eV could be attributed to the Fe²⁺ and Fe³⁺ species, respectively. In addition, there were two peaks in the Fe XPS spectra at binding energies of 715.2 and 719.0 eV, which corresponded to the satellite peaks of the Fe²⁺ and Fe³⁺, respectively [41]. Compared with 2% FeO_x/AC, the introduction of Pt caused partial Fe³⁺ to be reduced to Fe²⁺ and the binding energies for Fe 2p to be transferred to lower values with an increase of Pt loading. This indicated that the redox properties of Fe₃O₄ changed after introducing a small number of Pt species, confirming the interaction between Pt and FeO_x species [35]. The Fe²⁺/Fe³⁺ ratios estimated by XPS peak deconvolution increased with the increase of Pt loading, as shown in Table 1. Moreover, Figure 4b shows the Pt 4f XPS spectra for different catalysts; the Pt²⁺/Pt⁰ ratios are also shown in Table 1. After curve fitting, the spectrum consisted of two blue peaks

(71.3 and 74.7 eV) and two magenta peaks (72.4 and 75.6 eV), which could be assigned to Pt^0 and Pt^{2+} , respectively [42,43]. The binding energies for Pt 4f transferred to higher values with the increase of Fe loading, accordingly. When the loading of Fe was the same but with a decrease in the Pt/Fe molar ratio, the value of $\text{Pt}^{2+}/\text{Pt}^0$ increased, indicating that more electrons were transferred from Pt to Fe [38]. This further proves the electron transfer effect between Pt and Fe moieties due to the strong interaction. The XPS spectra of C and O are also presented in Figures S2 and S3. The peaks at 530.7, 531.8, 532.7, 533.7 and 535.0 eV were attributed to the lattice O of Fe–O, C=O, C–O, O–H and chemisorbed O+H₂O, respectively [44]. The C1s XPS spectra was shown in Figure S3, which can be deconvoluted into four C species, corresponding to CC (around 284.7 eV), C–O (around 285.3 eV), C=O (around 286.2 eV) and O–C=O (around 289.2 eV), respectively [45]. As shown in Table S1, for the fitted data, the proportion of Fe–O bond decreased with an increase of Pt loading, which may be attributed to the fact that Pt promoted the reduction of Fe species.

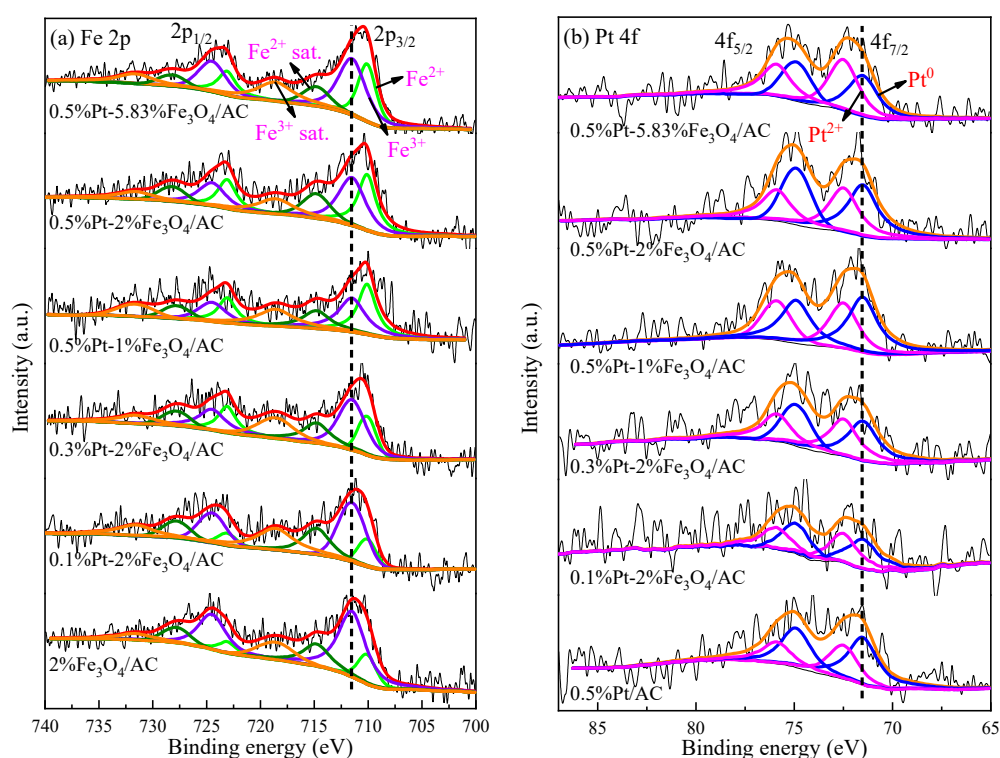


Figure 4. Fe 2p (a) and Pt 4f (b) XPS spectra of different catalysts.

Py-FTIR spectra were used to qualitatively and quantitatively analyze the Lewis and Brønsted acid. The peak at 1545 cm^{-1} was assigned to pyridine coordinated to the Brønsted acid sites (B), and the band at 1490 cm^{-1} was attributed to the overlap of Brønsted and Lewis acid sites (L) [46]. The characteristic infrared bands of adsorbed pyridine at Lewis acid sites (L) were observed at 1450 cm^{-1} and around 1600 cm^{-1} [47]. As shown in Figure 5, the catalyst samples contained a large number of Lewis acidic sites, while the Brønsted acidic sites at 1545 cm^{-1} were almost unobservable. Moreover, the Lewis acidic sites at 1450 cm^{-1} at a desorption temperature of $150\text{ }^\circ\text{C}$ were quantified; the data is presented in Table 1. It can be observed that the AC carrier had a certain number of Lewis acidic sites, and that the increase was not significant with the addition of small amounts of Pt or FeO_x . However, there was an obvious increase in Lewis acidic sites after the introduction of bimetallic Pt and FeO_x , and the Lewis acidic sites increased with increased Pt loading, which may be attributed to the fact that Pt promoted the reduction of iron oxide to form more unsaturated $\text{Fe}^{\delta+}$ with low coordination. Hence, the results of the Py-FTIR spectra

indicated that the synergy of Pt and FeO_x mainly increased the number of Lewis acidic sites that were conducive to the hydrogenolysis of C–O bonds for the catalyst [28].

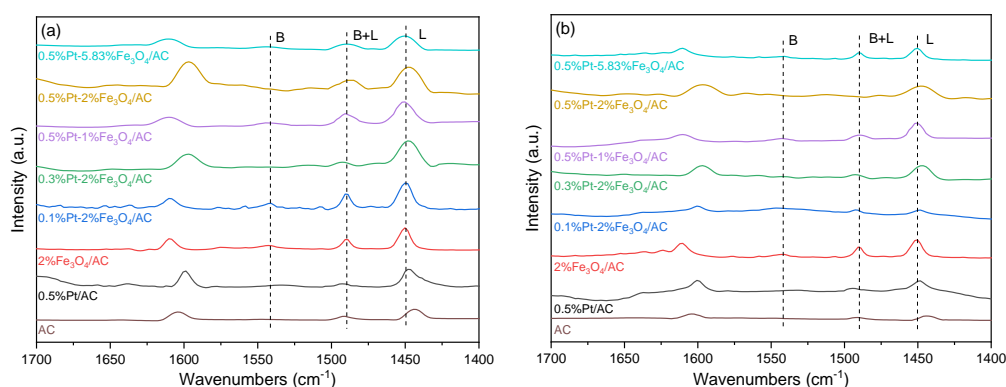


Figure 5. Py-FTIR spectra of different catalysts after pyridine adsorption at 50 °C and desorption at 150 °C (a) and 250 °C (b).

2.2. Catalytic Performance

The performance of different catalysts is summarized in Table 2. Without catalyst or with the use of a carbon support only, the conversion of HMF to DMF was extremely poor, i.e., below 10%, and no DMF was produced. Moreover, the 2% FeO_x/AC catalyst showed poor catalytic activity and carbon balance, with no DMF production, implying that Fe species alone have very poor hydrogenation ability. Based on previous literature, it was speculated that the relatively low carbon balance may have been due to the formation of condensation compounds [5,48]. When the 0.5% Pt/AC catalyst was used, the yield of DMF reached 36.1%, with 70.3% conversion of HMF within 2 h, with a small amount of over-hydrogenation byproduct DMTHF being formed, suggesting that Pt species were probably the essential active sites for selective hydrogenolysis of HMF to DMF. The catalytic performance of bimetallic catalysts with different loadings of Pt and Fe was also studied. It was found that no BHMF was detected in the reaction products of any of the catalysts, but a large amount of MF was present, indicating that HMF was first hydrogenolyzed to obtain MF on Pt-FeO_x/AC catalysts at 180 °C, and then hydrodeoxygenated to obtain DMF. As the Pt loading increased, the yield of DMF continued to increase. When the Pt loading was the same, little difference in the selectivity of DMF was observed, while the addition of a moderate amount of FeO_x facilitated the conversion of HMF. The higher HMF conversion was attributed to the fact that FeO_x improved the dispersion of Pt and increased the Lewis acidic sites. However, too much FeO_x caused the aggregation of Pt particles, resulting in inferior catalytic activity.

The effects of reaction parameters over 0.5% Pt-2% FeO_x/AC catalyst were investigated (Figure 6). As shown in Figure 6a, the effect of reaction temperature on the selective hydrogenolysis of HMF was studied. The reaction temperature played an extremely important role in the hydrodeoxygenation of HMF. At 100 °C, BHMF was observed as the main product; however, both BHMF and MF were observed at 140 °C. When the temperature was further increased to 160 °C, BHMF disappeared, but there was still 15.7% MF. This demonstrated the temperature dependent DMF formation pathway. The yield of DMF reached 75.8% at 180 °C and remained basically unchanged at higher temperatures. In addition, the carbon balance increased and then decreased with increasing temperature. According to our previous report, if the reaction temperature is too high, HMF is prone to coking [49], which affects the progress of the hydrodeoxygenation process. Moreover, the production of DMTHF, an overhydrogenation product of furan rings, also increased with an increase in reaction temperature.

Table 2. HMF hydrogenolysis to DMF over different catalysts.

Catalysts	HMF Conversion (mol %)	Yield (Selectivity) ^a (mol %)					Carbon Balance ^b (mol %)
		DMF	DMTHF	MF	MFA	BHMF	
0.5%Pt/AC	70.3	36.1 (51.3)	3.9 (5.5)	15.5 (22.0)	6.2 (8.8)	-	87.8
2%FeO _x /AC	30.7	-	-	2.4 (7.8)	-	-	7.8
0.1%Pt-2%FeO _x /AC	44.1	2.6 (5.9)	-	13.4 (30.3)	7.9 (17.9)	-	54.2
0.3%Pt-2%FeO _x /AC	56.2	8.1 (14.4)	-	26.4 (47.0)	11.1 (19.7)	-	81.1
0.5%Pt-1%FeO _x /AC	80.3	42.3 (52.7)	3.1 (3.9)	20.5 (25.5)	5.0 (6.2)	-	88.3
0.5%Pt-2%FeO _x /AC	86.4	46.5 (53.8)	-	23.8 (27.5)	7.6 (8.8)	-	90.2
0.5%Pt-5.83% FeO _x /AC	65.3	36.9 (56.5)	-	18.1 (27.7)	2.7 (4.1)	-	88.4

^a The data in brackets are the selectivity of product. ^b The carbon balance was the ratio of the carbon mole concentration of the detected products to the carbon mole concentration of the converted HMF. Reaction conditions: $T = 180\text{ }^{\circ}\text{C}$, $p(\text{H}_2) = 1.5\text{ MPa}$, $t = 2\text{ h}$, stirring speed = 600 rpm, $m_{\text{HMF}} = 250\text{ mg}$, $m_{\text{catalyst}} = 50\text{ mg}$, and $V_{\text{n-butanol}} = 20\text{ mL}$.

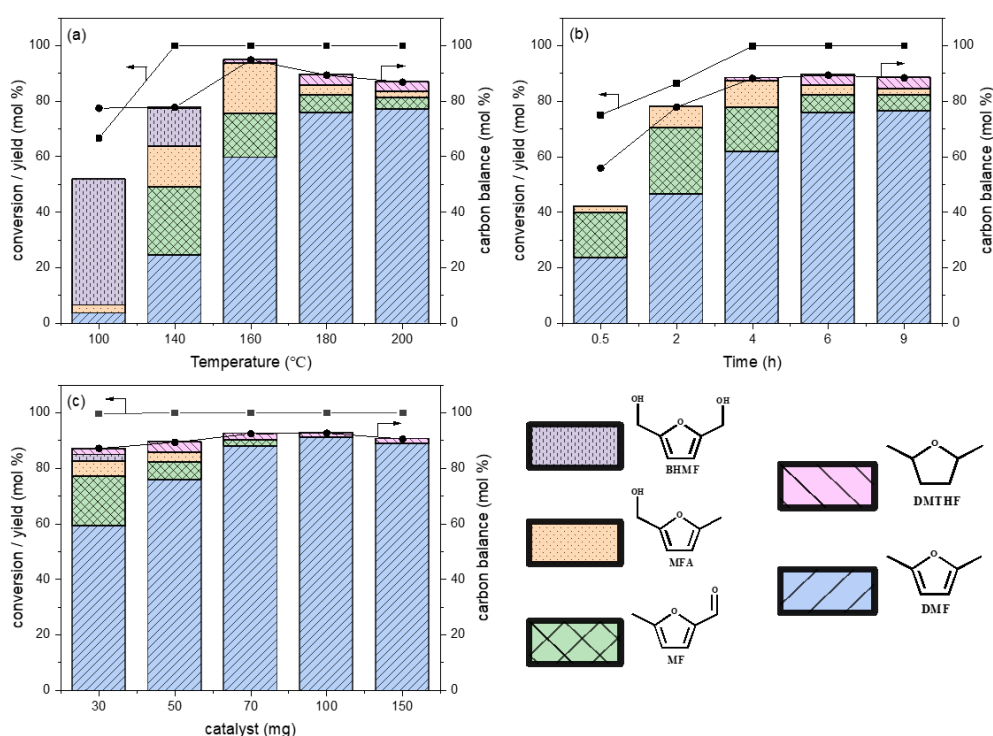


Figure 6. Effect of reaction temperature (a), reaction time (b) and catalyst loading (c) on HMF hydrogenolysis over 0.5% Pt-2% FeO_x/AC. Reaction conditions: (a) $P(\text{H}_2) = 1.5\text{ MPa}$, $t = 6\text{ h}$, stirring speed = 600 rpm, $m_{\text{HMF}} = 250\text{ mg}$, $m_{\text{catalyst}} = 50\text{ mg}$, $V_{\text{n-butanol}} = 20\text{ mL}$. (b) $T = 180\text{ }^{\circ}\text{C}$, $P(\text{H}_2) = 1.5\text{ MPa}$, stirring speed = 600 rpm, $m_{\text{HMF}} = 250\text{ mg}$, $m_{\text{catalyst}} = 50\text{ mg}$, $V_{\text{n-butanol}} = 20\text{ mL}$. (c) $T = 180\text{ }^{\circ}\text{C}$, $p(\text{H}_2) = 1.5\text{ MPa}$, $t = 6\text{ h}$, stirring speed = 600 rpm, $m_{\text{HMF}} = 250\text{ mg}$, $V_{\text{n-butanol}} = 20\text{ mL}$.

The effect of reaction time at $180\text{ }^{\circ}\text{C}$ was studied, and the results are shown in Figure 6b. The conversion of HMF increased with increasing reaction time, and complete conversion was achieved at 4 h. As time continued to increase, intermediate products MF and MFA were further converted into DMF, but the yield of DMF remained basically unchanged after 6 h. Figure 6c shows the conversion of HMF and product distribution with different catalyst loadings. When the loading of the catalyst was 30 mg, the conversion of HMF reached 99.7%, but the yield of DMF was only 59.1%, and there were still a large number of intermediate products such as MF. As catalyst loading increased from 30 to 100 mg, the number of active sites increased, resulting in an increase in the DMF yield. At 100 mg, the yield of DMF reached a maximum of 91.1%. However, further increasing the catalyst loading to 150 mg, the yield of DMF was nearly unchanged, indicating that the active sites with 100 mg catalyst were sufficient for the conversion of HMF. Moreover, the carbon balance

was basically maintained at around 90%. The yield of DMF reached a maximum of 91.1% at 180 °C for 6 h and 100 mg catalyst loading. Following a comparison with the literature, it was observed that the formation rate of DMF over a 0.5% Pt-2% FeO_x/AC catalyst was relatively high, and that the low loading of Pt presented an advantage considering the DMF yield and average reaction rate (Table S2).

Here, in order to explore the reaction pathway over a 0.5% Pt-2% FeO_x/AC catalyst, two controlled experiments were carried out using BHMF and MF intermediates as the feedstock (Table 3). When BHMF was used as the substrate, only 21.7% conversion was observed, and the DMF yield was only 9.5%. However, the yield of DMF reached 61.7% when MF was used as the substrate. Hence, it can be inferred that the hydroxyl group in HMF was first hydrodeoxygenated to form the MF intermediate, and then further hydrodeoxygenated to form DMF at 180 °C. This is consistent with the results obtained by analyzing the intermediate products at different temperatures and times. Generally, the selective hydrogenolysis of HMF is considered a pseudo-first-order reaction [49], and the activation energy of the intermediates was calculated according to the Arrhenius formula, as shown in Figure 7. It can be observed that the activation energy of MF (10.4 kJ/mol) is lower than that of BHMF (25.4 kJ/mol), further confirming that MF facilitates DMF formation in this reaction.

Table 3. Controlled experiments for DMF production from hydrogenolysis of intermediates.

Entry	Substrate	Conversion (mol %)	Product yield (mol %)		
			DMF	MF	MFA
1	BHMF	21.7	9.5	0	5.3
2	MF	82.5	61.7	17.5	19.4

Reaction conditions: $M_{\text{substrate}} = 2$ mmol, $m_{\text{catalyst}} = 100$ mg, $T = 180$ °C, $p(\text{H}_2) = 1.5$ MPa, $t = 1$ h, stirring speed = 600 rpm, and $V_{\text{n-butanol}} = 20$ mL.

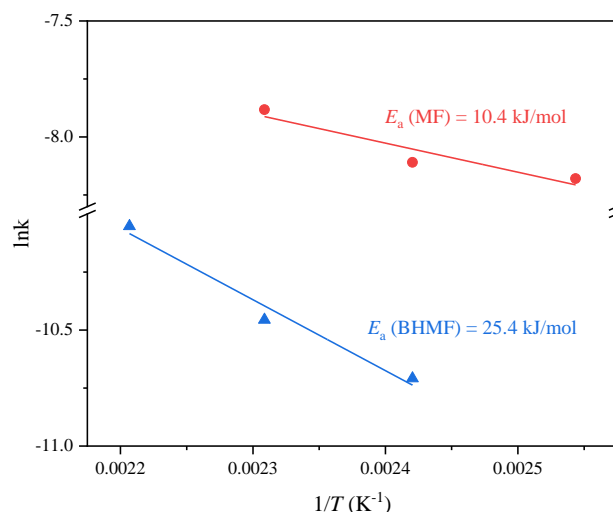
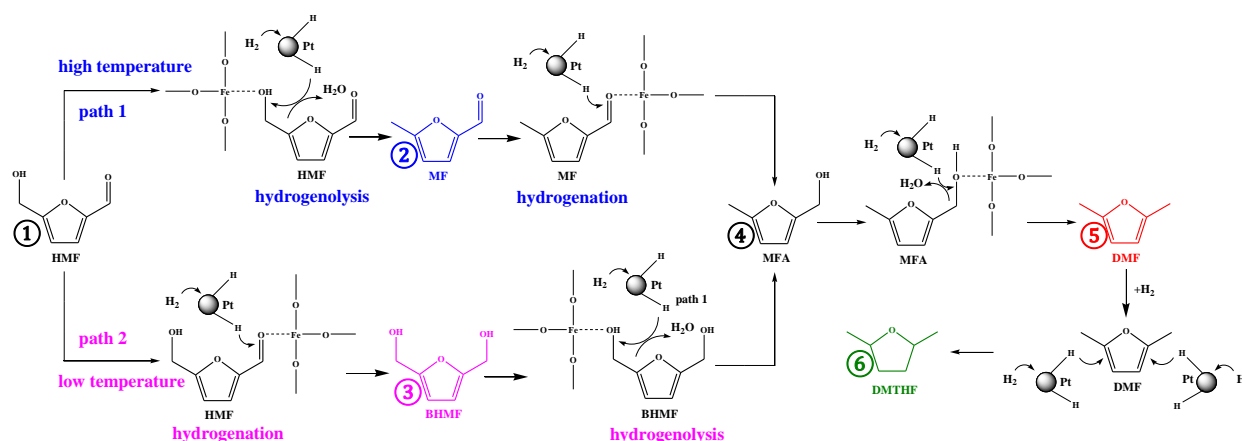


Figure 7. Profiles of Arrhenius plots of different intermediates in the selective hydrogenolysis of HMF over 0.5% Pt-2% FeO_x/AC.

The possible reaction mechanism is shown in Scheme 1, based on the synergistic effect of metal and Lewis acid, as we previously reported [49]. Generally, there are two pathways to produce DMF by selective hydrogenolysis of HMF, accompanied by the intermediates MF or BHMF, respectively. Path 1 is HMF hydrogenolysis at high temperature to MF intermediate. The activation of the C–OH groups in HMF occurred via the oxygen vacancies of acidic FeO_x species (Lewis acid), followed by splitting the C–O bond to form MF by the attacking of dissociated H atoms from the neighboring Pt. Then, the C=O bond in MF was adsorbed by the Lewis acidic sites of FeO_x for hydrogenation to MFA over Pt. Finally, the

hydroxyl group was further hydrogenolyzed to obtain the final product, DMF, through a similar synergistic effect of metal and Lewis acid as the first step. At low temperature, path 2 causes the first C=O hydrogenation of HMF to yield the BHMF intermediate, and then to produce DMF via the hydrogenolysis of two sequential hydroxyl groups of BHMF via a similar process of cooperative metal hydrogenation and acid activation.



Scheme 1. Reaction route for the hydrogenolysis of 5-hydroxymethylfurfural.

2.3. Catalyst Stability

The stability of the 0.5% Pt-2% FeO_x/AC catalyst for selective hydrogenolysis of HMF was investigated (Figure 8a). It was observed that the yield of DMF in the first three cycles decreased slightly. However, in the fourth cycle, the DMF yield decreased rapidly, and a large amount of excessive hydrogenation product, i.e., DMTHF, was formed. In order to explore the reasons for the deactivation of catalyst, the liquid product after the reaction was measured by ICP (Table 1); it was found that 28.5% of the Fe had leached into the solution after one reaction. As shown in Figure 9b, the characteristic peak of Fe₃O₄ decreased with the increase in the number of reaction runs, ultimately almost disappearing. Moreover, as shown in Figure 9, it was observed in the TEM image of the applied catalyst that the average Pt particle size increased slightly. The Fe, Pt, C and O XPS spectra for the applied catalysts are also shown in Figure S5. As the reaction run increased, Pt was gradually reduced to zero valence due to the presence of H₂ during the reaction, which is beneficial to the hydrogenation of C=C for furan saturation, while the Fe–O bond gradually disappeared, resulting in a larger proportion of C–O signals. This indicated that the loss of Fe species caused a metal–acid imbalance, thereby reducing the selectivity of DMF.

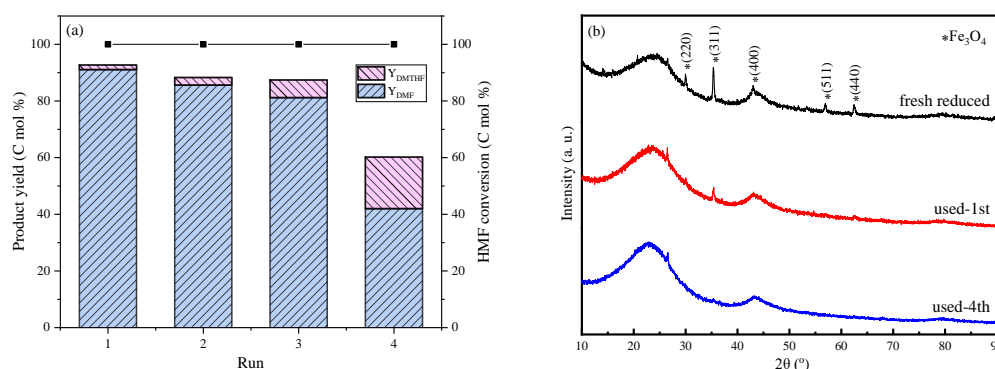


Figure 8. (a) Stability of 0.5% Pt-2% FeO_x/AC catalyst. Reaction conditions: $T = 180\text{ }^{\circ}\text{C}$, $p(\text{H}_2) = 1.5\text{ MPa}$, $t = 6\text{ h}$, stirring speed = 600 rpm, $m_{\text{HMF}} = 250\text{ mg}$, $m_{\text{catalyst}} = 100\text{ mg}$, $V_{n\text{-butanol}} = 20\text{ mL}$. (b) The XRD patterns of freshly-reduced, first-use and fourth-use 0.5% Pt-2% FeO_x/AC catalyst.

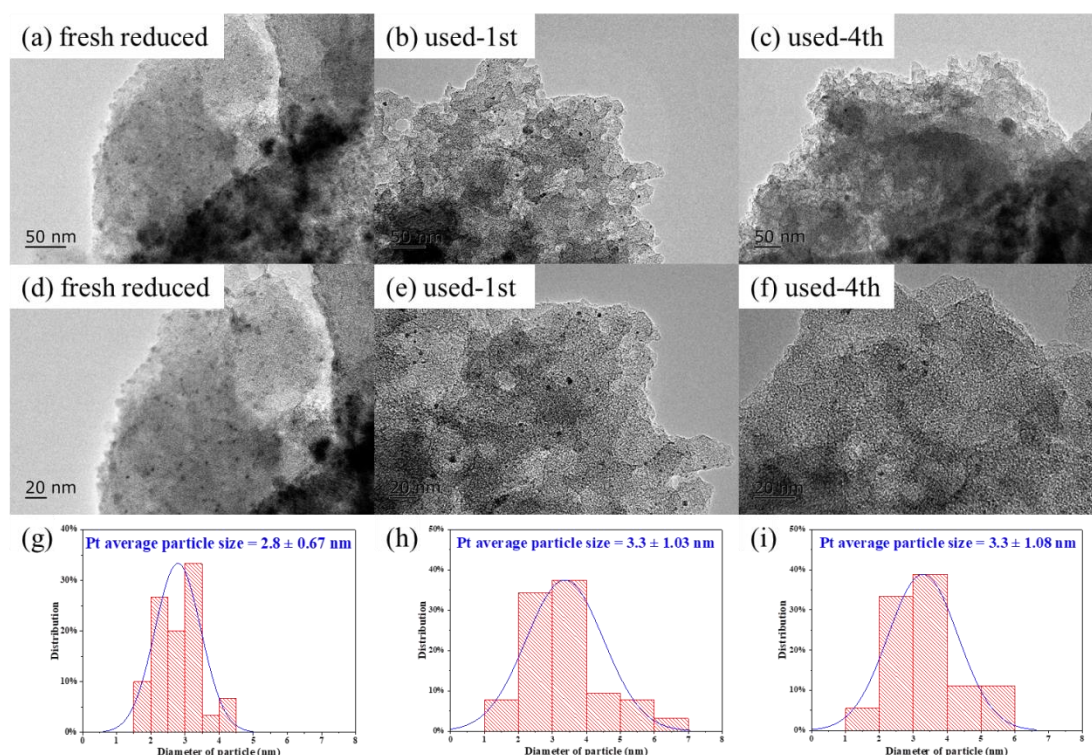


Figure 9. TEM images of freshly-reduced (a,d), first-use (b,e) and fourth-use (c,f) 0.5% Pt-2% FeO_x/AC; particle size distribution histogram of freshly-reduced (g), first-use (h) and fourth-use (i) 0.5% Pt-2% FeO_x/AC.

3. Materials and Methods

3.1. Materials

All materials were used without further purification. HMF, DMF, BHMF, 5-methylfurfural (MF), 5-methylfurfuryl alcohol (MFA) and 2,5-dimethyltetrahydrofuran (DMTHF) were purchased from Macklin Biochemical Co., Ltd. (Shanghai, China). H₂PtCl₆·6H₂O was obtained from Aladdin Reagent Co., Ltd. (Shanghai, China). Activated carbon (AC), Fe(NO₃)₃·9H₂O, n-butanol and cyclohexanone were purchased from Chemical Reagent Factory (Xi'an, China).

3.2. Catalysts Preparation

First, 0.5 g activated carbon (AC) and 0.0723 g Fe(NO₃)₃·9H₂O were mixed and ground for 10 min. Then, the black powder was annealed at 5500 °C for 4 h at a rate of 5 °C/min under nitrogen atmosphere. Next, 0.133 mL H₂PtCl₆ aqueous solution (0.05 g/mL H₂PtCl₆) and 10 mL deionized water were added to the prepared FeO_x/AC, and the mixed suspension was sonicated for 0.5 h and dried overnight at 100 °C. The dried black powder was annealed at 500 °C for 1 h at a rate of 5 °C/min under nitrogen atmosphere. The prepared 0.5% Pt-2% FeO_x/AC (0.5% and 2% represent the weight percentages of Pt and Fe, respectively) catalyst was reduced at 200 °C for 1 h under 40 mL/min hydrogen flow before reaction and characterization. Other catalysts with different loadings of Pt and Fe were prepared following a similar procedure.

3.3. Catalyst Characterization

XRD (X-ray diffraction) was used to identify the crystal structure of the sample; this was carried out on a X'Pert-ProMPD X-ray Diffractometer (PANalytical Company, Almelo, The Netherlands) with Cu K α radiation ($\lambda = 0.154$ nm). XPS (X-ray photoelectron spectroscopy) was used to analyze the valence and composition of catalysts; this was performed using a Escalab 250 Xi photoelectron spectrometer (Thermo Fisher Scientific Inc., Waltham, MA, USA) with Al K α radiation. The binding energies used C 1s at 284.8 eV

for calibration. The loadings (wt %) of Pt and Fe in the catalyst was analyzed using an Agilent 7900 inductively coupled plasma emission spectrometer (ICP-OES, Agilent Technologies, Santa Clara, CA, USA), and the leaching of Pt and Fe after the reaction was also measured by ICP-OES by following the same procedure. Transmission electron microscope (TEM) images were obtained on JEM-2100 (Japan) with an energy-dispersive X-ray spectrometer (Thermo Scientific UltraDry, Waltham, MA, USA) at 200 kV. Assuming that the Pt particles were spherical, their size distribution was obtained by counting the size of approximately 150 individual particles on the TEM image using the Digimizer software (V4.5.1, MedCalc Software Ltd., Ostend, Belgium, 2005). The average particle size was then calculated according to the equation: $d = \sum n_i d_i^3 / \sum n_i d_i^2$ [50,51]. A Nicolet 6700 infrared spectrometer (IR, Nicolet Instrument Company, Orlando, FL, USA) was used to determine the distribution of Brønsted (B) and Lewis (L) acidity in the catalysts. Prior to analysis, 50 mg sample was treated under vacuum (10^{-4} mmHg) at 200 °C for 0.5 h. After cooling to 50 °C, the IR spectra were recorded. Next, the sample was exposed to pyridine atmosphere for 15 min. Finally, the spectra were again recorded after vacuum desorption at 150 °C for 0.5 h, and the recorded background spectrum was subtracted. The number of Brønsted and Lewis acidic sites in the sample was analyzed by calculating the peak areas based on the absorption peaks at around ~ 1545 cm^{-1} and ~ 1450 cm^{-1} , respectively. The formulae, as described in, are as follows [52,53]:

$$C(\text{pyridine on B sites}) = 1.88 \text{ IA(B)} R^2 / W \quad (1)$$

$$C(\text{pyridine on L sites}) = 1.42 \text{ IA(L)} R^2 / W \quad (2)$$

C is the acid amount of catalyst (mmol/g catalyst), IA (B, L) is the absorbance integral of the B or L absorption peak, and R and W are the radius and mass of the self-supporting disc of the catalyst, respectively.

3.4. Catalytic Performance

A catalytic performance test was performed in a 70 mL autoclave with magnetic stirring. In a typical experiment, a reaction mixture of 250 mg HMF, 20 mL n-butanol and 50 mg freshly reduced 0.5% Pt-2% FeO_x/AC catalyst was added to the autoclave. Subsequently, the reactor was sealed and the air was removed by repeatedly filling and emptying with H₂ (five times). Afterwards, the reactor was pressurized to 1.5 MPa H₂ and heated to 180 °C. After a certain reaction time, the autoclave was cooled in ice water and the products were centrifuged to collect the supernatant. For the stability test, the centrifuged catalyst was collected after drying at 60 °C for 1 h, and then used directly in the next reaction. The products were analyzed by gas chromatography (GC-950, Haixin Chromatography Instruments Co., Shanghai, China) equipped with a flame-ionized detector and a KB-Wax capillary column (30 m × 0.32 mm × 0.5 μm). The quantification of the products was determined using cyclohexanone as the internal standard. All values were measured three times, and the error was within ±5%. The conversion of HMF and the product yield were defined as:

$$\text{HMF conversion (\%)} = \left(1 - \frac{\text{final moles of HMF}}{\text{initial moles of HMF}} \right) \times 100\% \quad (3)$$

$$\text{Product yield (\%)} = \frac{\text{moles of product (e. g., DMF)}}{\text{initial moles of HMF}} \times 100\% \quad (4)$$

4. Conclusions

A bimetallic Pt-FeO_x/AC catalyst was prepared by following a simple procedure, i.e., by loading Fe followed by Pt; the Pt was uniformly distributed on the support, with an average particle size of 2.8 nm. The addition of FeO_x not only improved the dispersion of Pt, but also increased the Lewis acidic sites. The Lewis acidic sites and adjacent Pt atoms were necessary for HMF hydrogenolysis to DMF via activation of C–O bonds over FeO_x

and hydrogenation over Pt, obtaining a maximal yield of DMF of 91.1% under optimal conditions. Reaction temperature could mediate the DMF formation pathway via the key intermediate, i.e., BHMF at low temperature and MF at high temperature.

Supplementary Materials: The following are available online at <https://www.mdpi.com/article/10.3390/catal11080915/s1>. Figure S1: TEM images and particle size distribution histogram of 0.1% Pt-2% FeO_x/AC (a,b), 0.3% Pt-2% FeO_x/AC (c,d), 0.5% Pt-1% FeO_x/AC (e,f), 0.5% Pt-5.83% FeO_x/AC (g,h), Figure S2: The O 1s XPS spectra of different catalysts, Figure S3: The C 1s XPS spectra of different catalysts, Table S1: The O 1s and C 1s XPS peak fitting data of different catalysts, Table S2: Reports on the hydrogenation of HMF to DMF over Pt based catalysts, Figure S4: Effect of H₂ pressure on HMF hydrogenolysis over 0.5% Pt-2% FeO_x/AC, Figure S5: The Fe 2p (a), Pt 4f (b), O 1s (c) and C 1s (d–f) XPS spectra of fresh reduced, used-1st and used-4th 0.5% Pt-2% FeO_x/AC catalyst.

Author Contributions: Conceptualization, S.L. (Shuang Li) and Q.L.; Data curation, Y.X., S.L. (Sichan Li), H.W. and Q.L.; Formal analysis, Y.X. and Q.L.; Funding acquisition, S.L. (Shuang Li) and Q.L.; Investigation, Y.X., S.L. (Sichan Li) and H.W.; Methodology, Y.X. and Q.L.; Project administration, S.L. (Shuang Li) and Q.L.; Resources, L.C., S.L. (Shuang Li) and Q.L.; Validation, S.L. (Shuang Li) and Q.L.; Writing—original draft, Y.X.; Writing—review & editing, H.W., S.L. (Shuang Li) and Q.L. All authors have read and agreed to the published version of the manuscript.

Funding: This work is financially supported by the National Key Research and Development Program of China (2018YFB1501402 and 2019YFD1100601) and the National Natural Science Foundation of China (51976220 and 21878244).

Data Availability Statement: Not Applicable.

Conflicts of Interest: The authors declare no conflict of interest.

References

1. Yang, F.; Mao, J.; Li, S.; Yin, J.; Zhou, J.; Liu, W. Cobalt–graphene nanomaterial as an efficient catalyst for selective hydrogenation of 5-hydroxymethylfurfural into 2,5-dimethylfuran. *Catal. Sci. Technol.* **2019**, *9*, 1329–1333. [CrossRef]
2. Tan, J.; Cui, J.; Zhu, Y.; Cui, X.; Shi, Y.; Yan, W.; Zhao, Y. Complete Aqueous Hydrogenation of 5-Hydroxymethylfurfural at Room Temperature over Bimetallic RuPd/Graphene Catalyst. *ACS Sustain. Chem. Eng.* **2019**, *7*, 10670–10678. [CrossRef]
3. Wang, H.; Zhu, C.; Li, D.; Liu, Q.; Tan, J.; Wang, C.; Cai, C.; Ma, L. Recent advances in catalytic conversion of biomass to 5-hydroxymethylfurfural and 2, 5-dimethylfuran. *Renew. Sustain. Energy Rev.* **2019**, *103*, 227–247. [CrossRef]
4. Fulignati, S.; Antonetti, C.; Licursi, D.; Pieraccioni, M.; Wilbers, E.; Heeres, H.J.; Raspolli Galletti, A.M. Insight into the hydrogenation of pure and crude HMF to furan diols using Ru/C as catalyst. *Appl. Catal. A* **2019**, *578*, 122–133. [CrossRef]
5. Zhang, Z.; Wang, C.; Gou, X.; Chen, H.; Chen, K.; Lu, X.; Ouyang, P.; Fu, J. Catalytic in-situ hydrogenation of 5-hydroxymethylfurfural to 2,5-dimethylfuran over Cu-based catalysts with methanol as a hydrogen donor. *Appl. Catal. A* **2019**, *570*, 245–250. [CrossRef]
6. Sarkar, C.; Koley, P.; Shown, I.; Lee, J.; Liao, Y.F.; An, K.; Tardio, J.; Nakka, L.; Chen, K.H.; Mondal, J. Integration of Interfacial and Alloy Effects to Modulate Catalytic Performance of Metal–Organic-Framework-Derived Cu–Pd Nanocrystals toward Hydrogenolysis of 5-Hydroxymethylfurfural. *ACS Sustain. Chem. Eng.* **2019**, *7*, 10349–10362. [CrossRef]
7. Yang, Y.; Liu, H.; Li, S.; Chen, C.; Wu, T.; Mei, Q.; Wang, Y.; Chen, B.; Liu, H.; Han, B. Hydrogenolysis of 5-Hydroxymethylfurfural to 2,5-Dimethylfuran under Mild Conditions without Any Additive. *ACS Sustain. Chem. Eng.* **2019**, *7*, 5711–5716. [CrossRef]
8. Li, J.; Song, Z.; Hou, Y.; Li, Z.; Xu, C.; Liu, C.; Dong, W. Direct Production of 2,5-Dimethylfuran with High Yield from Fructose over a Carbon-Based Solid Acid-Coated CuCo Bimetallic Catalyst. *ACS Appl. Mater. Interfaces* **2019**, *11*, 12481–12491. [CrossRef]
9. Solanki, B.S.; Rode, C.V. Selective hydrogenolysis of 5-(hydroxymethyl)furfural over Pd/C catalyst to 2,5-dimethylfuran. *J. Saudi Chem. Soc.* **2019**, *23*, 439–451. [CrossRef]
10. Zhang, Z.; Yao, S.; Wang, C.; Liu, M.; Zhang, F.; Hu, X.; Chen, H.; Gou, X.; Chen, K.; Zhu, Y.; et al. CuZnCoO_x multifunctional catalyst for in situ hydrogenation of 5-hydroxymethylfurfural with ethanol as hydrogen carrier. *J. Catal.* **2019**, *373*, 314–321. [CrossRef]
11. Talpade, A.D.; Tiwari, M.S.; Yadav, G.D. Selective hydrogenation of bio-based 5-hydroxymethyl furfural to 2,5-dimethylfuran over magnetically separable Fe-Pd/C bimetallic nanocatalyst. *Mol. Catal.* **2019**, *465*, 1–15. [CrossRef]
12. Hu, L.; Tang, X.; Xu, J.; Wu, Z.; Lin, L.; Liu, S. Selective Transformation of 5-Hydroxymethylfurfural into the Liquid Fuel 2,5-Dimethylfuran over Carbon-Supported Ruthenium. *Ind. Eng. Chem. Res.* **2014**, *53*, 3056–3064. [CrossRef]
13. Priece, P.; Endot, N.A.; Carà, P.D.; Lopez-Sanchez, J.A. Fast Catalytic Hydrogenation of 2,5-Hydroxymethylfurfural to 2,5-Dimethylfuran with Ruthenium on Carbon Nanotubes. *Ind. Eng. Chem. Res.* **2018**, *57*, 1991–2002. [CrossRef]
14. Luo, J.; Arroyo-Ramírez, L.; Gorte, R.J.; Tzoulaki, D.; Vlachos, D.G. Hydrodeoxygenation of HMF over Pt/C in a continuous flow reactor. *AIChE J.* **2015**, *61*, 590–597. [CrossRef]

15. Shi, J.; Wang, Y.; Yu, X.; Du, W.; Hou, Z. Production of 2,5-dimethylfuran from 5-hydroxymethylfurfural over reduced graphene oxides supported Pt catalyst under mild conditions. *Fuel* **2016**, *163*, 74–79. [[CrossRef](#)]
16. Chatterjee, M.; Ishizaka, T.; Kawanami, H. Hydrogenation of 5-hydroxymethylfurfural in supercritical carbon dioxide–water: A tunable approach to dimethylfuran selectivity. *Green Chem.* **2014**, *16*, 1543–1551. [[CrossRef](#)]
17. Gyngazova, M.S.; Negahdar, L.; Blumenthal, L.C.; Palkovits, R. Experimental and kinetic analysis of the liquid phase hydrodeoxygenation of 5-hydroxymethylfurfural to 2,5-dimethylfuran over carbon-supported nickel catalysts. *Chem. Eng. Sci.* **2017**, *173*, 455–464. [[CrossRef](#)]
18. Goyal, R.; Sarkar, B.; Bag, A.; Siddiqui, N.; Dumbre, D.; Lucas, N.; Bhargava, S.K.; Bordoloi, A. Studies of synergy between metal–support interfaces and selective hydrogenation of HMF to DMF in water. *J. Catal.* **2016**, *340*, 248–260. [[CrossRef](#)]
19. Li, D.; Liu, Q.; Zhu, C.; Wang, H.; Cui, C.; Wang, C.; Ma, L. Selective hydrogenolysis of 5-hydroxymethylfurfural to 2,5-dimethylfuran over Co_3O_4 catalyst by controlled reduction. *J. Energy Chem.* **2019**, *30*, 34–41. [[CrossRef](#)]
20. Hansen, T.S.; Barta, K.; Anastas, P.T.; Ford, P.C.; Riisager, A. One-pot reduction of 5-hydroxymethylfurfural via hydrogen transfer from supercritical methanol. *Green Chem.* **2012**, *14*, 2457–2461. [[CrossRef](#)]
21. Luo, J.; Lee, J.D.; Yun, H.; Wang, C.; Monai, M.; Murray, C.B.; Fornasiero, P.; Gorte, R.J. Base metal-Pt alloys: A general route to high selectivity and stability in the production of biofuels from HMF. *Appl. Catal. B* **2016**, *199*, 439–446. [[CrossRef](#)]
22. Esen, M.; Akmaz, S.; Koç, S.N.; Gürkaynak, M.A. The hydrogenation of 5-hydroxymethylfurfural (HMF) to 2,5-dimethylfuran (DMF) with sol–gel Ru-Co/ SiO_2 catalyst. *J. Sol.-Gel Sci. Technol.* **2019**, *91*, 664–672. [[CrossRef](#)]
23. Wang, G.; Hilgert, J.; Richter, F.H.; Wang, F.; Bongard, H.J.; Spliethoff, B.; Weidenthaler, C.; Schüth, F. Platinum–cobalt bimetallic nanoparticles in hollow carbon nanospheres for hydrogenolysis of 5-hydroxymethylfurfural. *Nat. Mater.* **2014**, *13*, 293–300. [[CrossRef](#)] [[PubMed](#)]
24. Nishimura, S.; Ikeda, N.; Ebitani, K. Selective hydrogenation of biomass-derived 5-hydroxymethylfurfural (HMF) to 2,5-dimethylfuran (DMF) under atmospheric hydrogen pressure over carbon supported PdAu bimetallic catalyst. *Catal. Today* **2014**, *232*, 89–98. [[CrossRef](#)]
25. Zhang, F.; Liu, Y.; Yuan, F.; Niu, X.; Zhu, Y. Efficient Production of the Liquid Fuel 2,5-Dimethylfuran from 5-Hydroxymethylfurfural in the Absence of Acid Additive over Bimetallic PdAu Supported on Graphitized Carbon. *Energy Fuels* **2017**, *31*, 6364–6373. [[CrossRef](#)]
26. Gawade, A.B.; Tiwari, M.S.; Yadav, G.D. Biobased Green Process: Selective Hydrogenation of 5-Hydroxymethylfurfural to 2,5-Dimethyl Furan under Mild Conditions Using Pd-Cs_{2.5}H_{0.5}PW₁₂O₄₀/K-10 Clay. *ACS Sustain. Chem. Eng.* **2016**, *4*, 4113–4123. [[CrossRef](#)]
27. Yang, Y.; Liu, Q.; Cai, C.; Tan, J.; Wang, T.; Ma, L. Advances in DMF and C₅/C₆ Alkanes Production from Lignocellulose. *Prog. Chem.* **2016**, *28*, 363–374.
28. Yang, Y.; Liu, Q.; Li, D.; Tan, J.; Zhang, Q.; Wang, C.; Ma, L. Selective hydrodeoxygenation of 5-hydroxymethylfurfural to 2,5-dimethylfuran on Ru–MoO_x/C catalysts. *RSC Adv.* **2017**, *7*, 16311–16318. [[CrossRef](#)]
29. Zhang, L.; Zhou, M.; Wang, A.; Zhang, T. Selective Hydrogenation over Supported Metal Catalysts: From Nanoparticles to Single Atoms. *Chem. Rev.* **2019**, *120*, 683–733. [[CrossRef](#)]
30. Wang, X.; Liang, X.; Li, J.; Li, Q. Catalytic hydrogenolysis of biomass-derived 5-hydroxymethylfurfural to biofuel 2, 5-dimethylfuran. *Appl. Catal. A* **2019**, *576*, 85–95. [[CrossRef](#)]
31. Yu, L.; He, L.; Chen, J.; Zheng, J.; Ye, L.; Lin, H.; Yuan, Y. Robust and Recyclable Nonprecious Bimetallic Nanoparticles on Carbon Nanotubes for the Hydrogenation and Hydrogenolysis of 5-Hydroxymethylfurfural. *ChemCatChem* **2015**, *7*, 1701–1707. [[CrossRef](#)]
32. Shi, Y.; Yuan, Z.; Wei, Q.; Sun, K.; Xu, B. Pt–FeO_x/SiO₂ catalysts prepared by galvanic displacement show high selectivity for cinnamyl alcohol production in the chemoselective hydrogenation of cinnamaldehyde. *Catal. Sci. Technol.* **2016**, *6*, 7033–7037. [[CrossRef](#)]
33. Wan, W.; Jiang, Z.; Chen, J.G. A Comparative Study of Hydrodeoxygenation of Furfural Over Fe/Pt(111) and Fe/Mo₂C Surfaces. *Top. Catal.* **2018**, *61*, 439–445. [[CrossRef](#)]
34. Zanuttini, M.S.; Gross, M.; Marchetti, G.; Querini, C. Furfural hydrodeoxygenation on iron and platinum catalysts. *Appl. Catal. A* **2019**, *587*, 117217. [[CrossRef](#)]
35. Cui, W.; Xue, D.; Tan, N.; Zheng, B.; Jia, M.; Zhang, W. Pt supported on octahedral Fe₃O₄ microcrystals as a catalyst for removal of formaldehyde under ambient conditions. *Chin. J. Catal.* **2018**, *39*, 1534–1542.
36. Guo, C.; Lu, W.; Wei, G.; Jiang, L.; Yu, Y.; Hu, Y. Formation of 1D chain-like Fe₃O₄@C/Pt sandwich nanocomposites and their magnetically recyclable catalytic property. *Appl. Surf. Sci.* **2018**, *457*, 1136–1141. [[CrossRef](#)]
37. Liu, H.; Tian, K.; Ning, J.; Zhong, Y.; Zhang, Z.; Hu, Y. One-Step Solvothermal Formation of Pt Nanoparticles Decorated Pt²⁺-Doped α -Fe₂O₃ Nanoplates with Enhanced Photocatalytic O₂ Evolution. *ACS Catal.* **2019**, *9*, 1211–1219. [[CrossRef](#)]
38. Pan, H.; Li, J.; Lu, J.; Wang, G.; Xie, W.; Wu, P.; Li, X. Selective hydrogenation of cinnamaldehyde with PtFe/Al₂O₃@SBA-15 catalyst: Enhancement in activity and selectivity to unsaturated alcohol by Pt–FeO_x and Pt–Al₂O₃@SBA-15 interaction. *J. Catal.* **2017**, *354*, 24–36. [[CrossRef](#)]
39. Wei, M.; Han, Y.; Liu, Y.; Su, B.; Yang, H.; Lei, Z. Green preparation of Fe₃O₄ coral-like nanomaterials with outstanding magnetic and OER properties. *J. Alloys Compd.* **2020**, *831*, 154702. [[CrossRef](#)]
40. Zhou, C.; Shi, W.; Wan, X.; Meng, Y.; Yao, Y.; Guo, Z.; Dai, Y.; Wang, C.; Yang, Y. Oxidation of 5-hydroxymethylfurfural over a magnetic iron oxide decorated rGO supporting Pt nanocatalyst. *Catal. Today* **2019**, *330*, 92–100. [[CrossRef](#)]

41. Neumann, S.; Doebler, H.H.; Keil, S.; Erdt, A.J.; Gutsche, C.; Borchert, H.; Kolny-Olesiak, J.; Parisi, J.; Bäumer, M.; Kunz, S. Effects of Particle Size on Strong Metal–Support Interactions Using Colloidal “Surfactant-Free” Pt Nanoparticles Supported on Fe₃O₄. *ACS Catal.* **2020**, *10*, 4136–4150. [[CrossRef](#)]
42. Sarno, M.; Ponticorvo, E. Much enhanced electrocatalysis of Pt/PtO₂ and low platinum loading Pt/PtO₂-Fe₃O₄ dumbbell nanoparticles. *Int. J. Hydrogen Energy* **2017**, *42*, 23631–23638. [[CrossRef](#)]
43. Tian, M.; Liu, S.; Wang, L.; Ding, H.; Zhao, D.; Wang, Y.; Cui, J.; Fu, J.; Shang, J.; Li, G.K. Complete Degradation of Gaseous Methanol over Pt/FeO_x Catalysts by Normal Temperature Catalytic Ozonation. *Environ. Sci. Technol.* **2020**, *54*, 1938–1945. [[CrossRef](#)]
44. Zhou, J.; Zhang, C.; Niu, T.; Huang, R.; Li, S.; Sun, J.; Wang, Y. Facile synthesis of reusable magnetic Fe/Fe₃C/C composites from renewable resources for super-fast removal of organic dyes: Characterization, mechanism and kinetics. *Powder Technol.* **2019**, *351*, 314–324. [[CrossRef](#)]
45. Yang, S.; Chen, L.; Mu, L.; Hao, B.; Chen, J.; Ma, P. Graphene foam with hierarchical structures for the removal of organic pollutants from water. *RSC Adv.* **2016**, *6*, 4889–4898. [[CrossRef](#)]
46. Fedyna, M.; Zak, A.; Jaroszevska, K.; Mokrzycki, J.; Trawczyński, J. Composite of Pt/AlSBA-15+zeolite catalyst for the hydroisomerization of n-hexadecane: The effect of platinum precursor. *Microporous Mesoporous Mater.* **2020**, *305*, 110366. [[CrossRef](#)]
47. Jystad, A.; Leblanc, H.; Caricato, M. Surface Acidity Characterization of Metal-Doped Amorphous Silicates via Py-FTIR and 15N NMR Simulations. *J. Phys. Chem. C* **2020**, *124*, 15231–15240. [[CrossRef](#)]
48. Li, J.; Zhang, J.; Liu, H.; Liu, J.; Xu, G.; Liu, J.; Sun, H.; Fu, Y. Graphitic Carbon Nitride (g-C₃N₄)-derived Fe-N-C Catalysts for Selective Hydrodeoxygenation of 5-Hydroxymethylfurfural to 2,5-Dimethylfuran. *ChemistrySelect* **2017**, *2*, 11062–11070. [[CrossRef](#)]
49. Zhu, C.; Wang, H.; Li, H.; Cai, B.; Lv, W.; Cai, C.; Wang, C.; Yan, L.; Liu, Q.; Ma, L. Selective Hydrodeoxygenation of 5-Hydroxymethylfurfural to 2,5-Dimethylfuran over Alloyed Cu–Ni Encapsulated in Biochar Catalysts. *ACS Sustain. Chem. Eng.* **2019**, *7*, 19556–19569. [[CrossRef](#)]
50. Simonsen, S.B.; Chorkendorff, I.; Dahl, S.; Skoglundh, M.; Sehested, J.; Helveg, S. Ostwald ripening in a Pt/SiO₂ model catalyst studied by in situ TEM. *J. Catal.* **2011**, *281*, 147–155. [[CrossRef](#)]
51. Shao, M.; Hu, C.; Xu, X.; Song, Y.; Zhu, Q. Pt/TS-1 catalysts: Effect of the platinum loading method on the dehydrogenation of n-butane. *Appl. Catal. A* **2021**, *621*, 118194. [[CrossRef](#)]
52. Emeis, C.A. Determination of intergrated molar extinction coefficients for infrared adsorption bands of pyridine adsorbed on solid acid catalysts. *J. Catal.* **1993**, *141*, 347–354. [[CrossRef](#)]
53. Ning, P.; Song, Z.; Li, H.; Zhang, Q.; Liu, X.; Zhang, J.; Tang, X.; Huang, Z. Selective catalytic reduction of NO with NH₃ over CeO₂-ZrO₂-WO₃ catalysts prepared by different methods. *Appl. Surf. Sci.* **2015**, *332*, 130–137. [[CrossRef](#)]